

# ESTIMATION OF DIVERGENCE-FREE 3D CARDIAC BLOOD FLOW IN A ZEBRAFISH LARVA USING MULTI-VIEW MICROSCOPY

Kevin G. Chan<sup>1</sup>     Michael Liebling<sup>1,2</sup>

<sup>1</sup>Electrical & Computer Engineering, University of California, Santa Barbara, CA 93106, USA

<sup>2</sup>Idiap Research Institute, CH-1920 Martigny, Switzerland

## ABSTRACT

Conventional fluid flow estimation methods for in vivo optical microscopy are limited to two-dimensions and are only able to estimate the components of flow parallel to the imaging plane. This limits the study of flow in more intricate biological structures, such as the embryonic zebrafish heart, where flow is three-dimensional. To measure three-dimensional blood flow, we propose an algorithm to reconstruct a 3D, divergence-free flow map from multiple 2D flow estimates computed from image stacks captured from different views. This allows us to estimate the out-of-plane velocity component that is normally lost with single-view imaging. This paper describes our 3D flow reconstruction algorithm, evaluates its performance on a simulated velocity field, and demonstrates its application to in vivo cardiac imaging within a live zebrafish larva.

*Index Terms*— 3D blood flow estimation, divergence-free flow, multi-view microscopy, optical microscopy

## 1. INTRODUCTION

Blood flow in the embryonic heart plays a critical role to ensure normal development, and perturbations to the normal flow can lead to severe heart defects [1]. Measuring these flows in 3D has remained a challenge due to the limited acquisition speed of conventional 3D imaging modalities and the rapid motion of blood cells in the heart. New microscope designs using electrically tunable lenses have begun to address this issue and have demonstrated acquisition rates of up to 30 volumes per second [2]. However, such designs require a tradeoff between temporal and axial sampling, so increasing the number of volumes per second is only possible by taking volumes with fewer  $z$ -slices. In optical microscopy, blood flow estimation is typically performed on 2D video sequences acquired at very high frame rates (400-1000 frames per second for zebrafish) [1, 3]. However, this 2D approach is only able to measure the components of velocity parallel to the acquisition plane, and any out-of-plane motion is lost, as illustrated in Fig. 1(a-c).

A number of methods have recently been proposed to recover three-dimensional flow with MRI [4, 5] and ultrasound imaging [6]. Unfortunately, these imaging modalities often

lack the spatio-temporal resolution necessary for imaging blood flow in small organisms and developing embryos. In comparison, optical microscopy offers high resolution and allows use of fluorescent probes to image specific biological structures and functions of interest. Several 3D particle image velocimetry (PIV) methods have also been proposed, including holographic PIV [7] and defocusing PIV [8]. However, these methods have yet to be demonstrated with in vivo microscopy to measure 3D blood flow.

In this paper, we present a method to reconstruct 3D, divergence-free flow fields from multiple 2D projections acquired from different rotated views (e.g.  $0^\circ$  and  $90^\circ$  as shown in Fig. 1(d)). At a high level, our method is similar to the multi-view, divergence-free method used by Liu et al. to measure 3D motion of muscle tissue using MRI [9]. Our method also has similarities with other multi-view flow reconstruction methods [10, 11] that formulate the reconstruction problem as a constrained and regularized inverse problem. Unlike these methods, however, we do not use explicit constraints or separate regularization terms, but rather we directly reconstruct flow fields using radial basis functions which guarantee our reconstructed flow to be divergence-free, a common assumption for flow estimation. This also allows us to represent the 3D flow field with relatively few coefficients, making the method computationally tractable.

This paper is organized as follows. In Section 2, we present the multi-view 3D flow reconstruction method as a quadratic minimization problem. In Section 3, we evaluate our method using a simulated flow field. In Section 4, we discuss the experimental acquisition procedure and demonstrate our approach with in vivo microscopy to produce volumetric maps of 3D blood flow in the beating heart of a developing zebrafish larva.

## 2. PROBLEM FORMATION

Given a three-dimensional vector field  $\mathbf{v}(\mathbf{x}, t)$ , at every position  $\mathbf{x} \in \mathbb{R}^3$ , we consider orthogonal projections of this vector field onto  $K$  different planes:

$$\mathbf{v}_{\mathbf{n}_k}(\mathbf{x}, t) = \mathbf{P}_{\mathbf{n}_k} \{ \mathbf{v}(\mathbf{x}, t) \} \quad (1)$$

$$= \mathbf{v}(\mathbf{x}, t) - \langle \mathbf{v}(\mathbf{x}, t), \mathbf{n}_k \rangle \mathbf{n}_k, \quad (2)$$

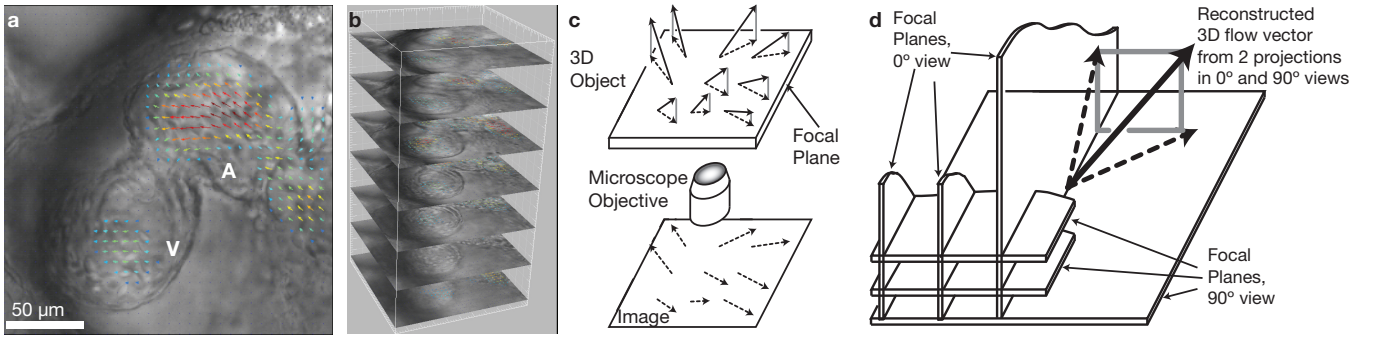


**Fig. 1.** (a) Still frame of a high-speed video of the beating heart in a larval zebrafish (A: atrium, V: ventricle). Blood flow was estimated using an optical flow technique. (b) 2D flow can be estimated at multiple depths in the sample by adjusting the focal plane. (c) Flow estimation algorithms can only recover the in-plane component (projection, dashed arrows) of the true velocity vector (black arrows). The out-of-plane component (gray line connecting the in-plane and true velocity vectors) is inaccessible. (d) The out-of-plane component can be measured by imaging the object from a different view (e.g. 90°).

where  $\mathbf{P}_{\mathbf{n}_k}\{\cdot\}$  is an operator that projects a vector onto the plane with unit normal vector  $\mathbf{n}_k$ ,  $\langle \cdot, \cdot \rangle$  is an inner product between two vectors, and  $k = 1, \dots, K$ . This situation reflects estimation of 2D flow within imaging planes, ignoring out-of-plane flow.

From these projections  $\mathbf{v}_{\mathbf{n}_k}(\mathbf{x}, t)$ , we aim to recover the 3D vector field  $\mathbf{v}(\mathbf{x}, t)$  with the following minimization:

$$\hat{\mathbf{v}}(\mathbf{x}, t) = \arg \min_{\hat{\mathbf{v}}(\mathbf{x}, t)} \sum_{k=1}^K (\mathbf{P}_{\mathbf{n}_k}\{\hat{\mathbf{v}}(\mathbf{x}, t)\} - \mathbf{v}_{\mathbf{n}_k}(\mathbf{x}, t))^2. \quad (3)$$

This equation ensures data consistency, i.e. the least-squares error is minimized when the projected estimate matches the measured field. However, we also wish to enforce fluid incompressibility in our flow reconstruction. Using a divergence-free interpolation method based on radial basis functions [12], we require that  $\hat{\mathbf{v}}(\mathbf{x}, t)$  satisfy

$$\hat{\mathbf{v}}(\mathbf{x}, t) = \sum_{j=1}^M \Phi(\mathbf{x} - \mathbf{m}_j) \mathbf{c}_j(t), \quad (4)$$

where  $\mathbf{c}_j$  ( $j = 1, \dots, M$ ) are vectorial radial basis coefficients,  $\mathbf{m}_j$  are their corresponding node locations, and  $\Phi$  is a matrix-valued radial basis function given by

$$\Phi(\mathbf{r}) = \left[ \left( 1 - \frac{\|\mathbf{r}\|^2}{2\alpha^2} \right) \mathbf{I} + \frac{1}{2\alpha^2} \mathbf{r}\mathbf{r}^\top \right] e^{-\frac{\|\mathbf{r}\|^2}{2\alpha^2}}, \quad (5)$$

where  $\mathbf{I}$  is the identity matrix, and  $\alpha$  is a real, positive-valued parameter that controls the smoothness of the vector field.

Combining Eqs. (3) and (4), we obtain the following modified minimization:

$$\hat{\mathbf{c}}_j(t) = \arg \min_{\mathbf{c}_j(t)} \sum_{k=1}^K \left( \mathbf{P}_{\mathbf{n}_k} \left\{ \sum_{j=1}^M \Phi(\mathbf{x} - \mathbf{m}_j) \mathbf{c}_j(t) \right\} - \mathbf{v}_{\mathbf{n}_k}(\mathbf{x}, t) \right)^2, \quad (6)$$

which can be solved using the conjugate gradient method. This minimization equation solves for the vectorial radial basis coefficients that produce the 3D vector field best matching our observed vector projections. After solving for the divergence-free coefficients  $\hat{\mathbf{c}}_j(t)$ , the 3D vector field can be interpolated using Eq. (4).

### 3. SIMULATION

We evaluated our method using the following divergence-free vector field:

$$\mathbf{v}(\mathbf{x}) = \begin{bmatrix} \gamma_1 yz \\ \gamma_1 xz \\ \gamma_2 \cos(\gamma_3(x+y)) \end{bmatrix}, \quad (7)$$

sampled on a  $10 \times 10 \times 10$  grid from  $-1$  mm to  $1$  mm in each direction (Fig. 2(a)), and where  $\gamma_1, \gamma_2, \gamma_3$  are constants such that  $\mathbf{v}(\mathbf{x})$  is in units of mm/s. Specifically,  $\gamma_1 = 1 \text{ mm}^{-1} \cdot \text{s}^{-1}$ ,  $\gamma_2 = 1 \text{ mm} \cdot \text{s}^{-1}$ , and  $\gamma_3 = 1 \text{ mm}^{-1}$ . We computed two  $10 \times 10 \times 10$  focal stacks from two different views of this vector field: one where vectors were projected onto slices parallel to the  $xy$ -plane (Fig. 2(b)) and one where vectors were projected onto slices with normal vector  $\mathbf{n} = [-\sin(45^\circ), 0, \cos(45^\circ)]^\top$ , corresponding to a  $45^\circ$  rotation of the  $xy$ -plane about the  $y$ -axis (Fig. 2(c)). In each view, we added zero-mean white Gaussian noise to both the magnitude and phase of the projected vectors. The standard deviation of the magnitude and phase noise are, respectively,  $\sigma_{\text{mag}} = 0.05 \text{ mm/s}$  and  $\sigma_\phi = 45^\circ$ . From these two views, we were able to recover the 3D vector field (shown in Fig. 2(d)) with a total mean squared error (for all three vector components) of  $0.13 \text{ mm/s}$ . All vector fields were visualized using ParaView 4.2.0 [13].

Additionally, we explored how the angle between different views affected the reconstruction accuracy. Using again

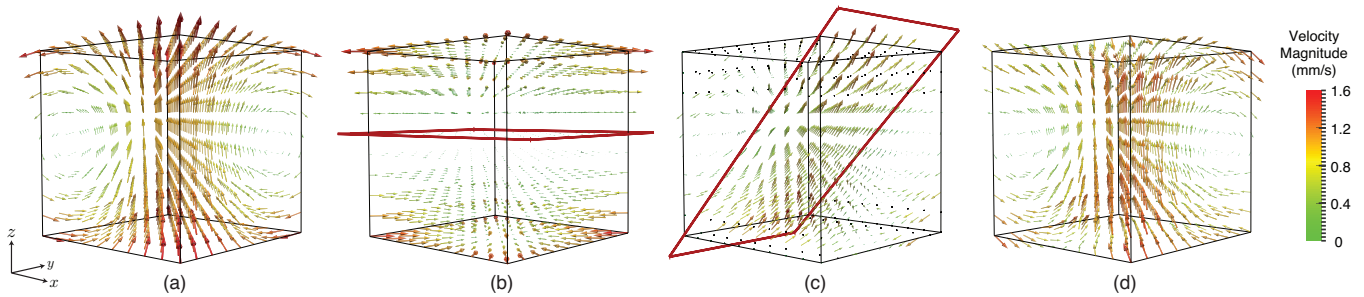


**Fig. 2.** (a) A  $10 \times 10 \times 10$  3D divergence-free velocity field is simulated. (b,c) We compute  $10 \times 10 \times 10$  focal stacks from two views of this velocity field, rotated by  $45^\circ$ . In each view, the 3D vectors on each focal slice are projected onto that 2D focal plane. In each stack, the center slice is outlined in red. (d) Our method is able to combine these two views to reconstruct the original 3D velocity field with a mean squared error of 0.13 mm/s.

the vector field given in Eq. 7 and taking two views separated by an angle  $\theta$ , we applied our method to reconstruct a 3D vector field. We repeated this with different values of  $\theta$  and found mean squared errors of 0.17 mm/s, 0.14 mm/s, and 0.06 mm/s for  $\theta = 15^\circ, 30^\circ, 90^\circ$ , respectively. Unsurprisingly, as  $\theta$  approaches  $90^\circ$ , the mean squared error decreases. This suggests that, in a 3D flow imaging experiment, it is ideal to acquire data from orthogonal views. When this is not possible (due to a lack of optical access), it is advisable to take views with the largest separation angle possible.

## 4. EXPERIMENTS

### 4.1. Acquisition

To demonstrate our method with in vivo microscopy, we immersed a 60 hpf (hours post fertilization) zebrafish larva in a 1.2% low melting point agarose, 0.016% tricaine (MS-222) solution and placed it inside a tube made of fluorinated ethylene propylene (FEP) which has a refractive index close to that of water. We then placed this tube on the stage of a Leica DMI6000B inverted microscope equipped with an HCX PL S-APO  $20\times/0.50$  dry objective. The tube was oriented perpendicular to the optical axis, and its axis of rotation was aligned parallel to the  $y$ -axis of the focal plane. Using a stepper motor, we rotated the tube to image the zebrafish heart from three different views, each rotated by an additional  $18^\circ$ . At each view, we acquired movies with  $512 \times 512$  pixels at 500 frames per second, covering 3 heartbeats, at 10 different  $z$ -slices with  $15 \mu\text{m}$  between each slice. After acquisition, we computationally synchronized the movies and extracted a channel containing only blood cells using the algorithm described in [3]. We then estimated flow velocity vectors (parallel to the imaging plane) at each  $z$ -slice using the Lucas-Kanade optical flow algorithm [14], as implemented in FlowJ [15]. Fig. 3 shows an example of 2D velocities estimated from three different views (for visibility, only a single plane is shown for each view).

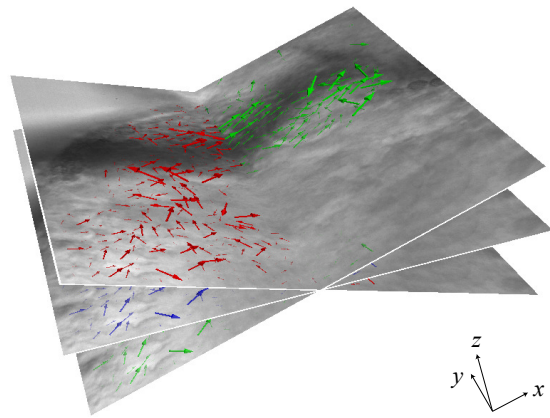


**Fig. 3.** We acquired focal stacks of the zebrafish heart from three views:  $-18^\circ, 0^\circ$ , and  $18^\circ$  relative to the  $xy$ -plane and rotated about the  $y$ -axis. At each view, 2D optical flow was used to estimate velocity vectors in each plane. For visibility, a single slice is shown for each view.

### 4.2. 3D Cardiac Flow Reconstruction

After estimating all 2D velocity fields, we estimated the 3D velocity field using the algorithm described in Section 2. We obtained a set of  $8 \times 8 \times 4$  uniformly spaced vector coefficients from the minimization in Eq. 6 and used it to interpolate the 3D velocity field onto a  $128 \times 128 \times 64$  grid. Fig. 4 shows the reconstructed blood flow velocity field during the atrial contraction phase of the heart. For a 60 hpf zebrafish embryo, we observed a maximum blood flow velocity of approximately 4 mm/s as blood is pumped from the atrium to the ventricle. This value falls between the maximum AV velocities of 0.9 mm/s and 5 mm/s for a 37 hpf and 4.5 dpf (days post fertilization) embryo, respectively, measured by Hove et al. [1]. We repeated this procedure at all timepoints to characterize three-dimensional blood flow over an entire cardiac cycle (see supplementary Movie 1).

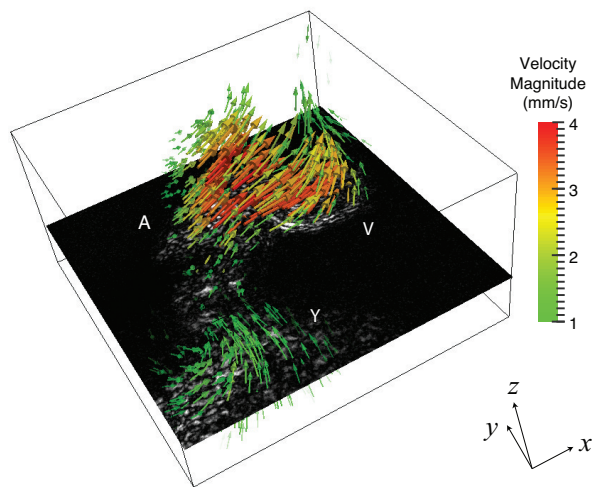


**Fig. 4.** We combine 2D flow estimates from three different views to recover a divergence-free 3D velocity map of blood flow through the heart of a zebrafish larva (A: atrium, V: ventricle, Y: yolk).

## 5. DISCUSSION

Since blood flow is inherently three-dimensional, current 2D imaging methods, which cannot measure out-of-plane motion, are inadequate to fully characterize complex flow trajectories. Multi-view imaging allows one to recover the out-of-plane component of motion and measure 3D flow. In this paper, we demonstrate a new method for combining multi-view 2D flow estimates to recover a divergence-free, 3D flow field. Since our method starts from 2D vector fields, we rely on accurate 2D flow separation and motion estimation algorithms as a pre-processing step. Additionally, since the normal vectors  $\mathbf{n}_k$  are assumed to be known, any rotational imperfections could also result in errors in the recovered 3D flow. This may be resolved with careful calibration, better volumetric image registration, or perhaps by including the projection angles (the normal vectors) into the optimization framework itself. We foresee our method to be applicable to not only transmitted light microscopy, but also to other modalities such as fluorescence microscopy (with fluorescently labeled blood cells).

## 6. REFERENCES

- [1] J.R. Hove, R.W. Koster, A.S. Forouhar, G. Acevedo-Bolton, S.E. Fraser, and M. Gharib, “Intracardiac fluid forces are an essential epigenetic factor for embryonic cardiogenesis,” *Nature*, vol. 421, no. 6919, pp. 172–177, Jan. 2003.
- [2] F.O. Fahrbach, F.F. Voigt, B. Schmid, F. Helmchen, and J. Huisken, “Rapid 3D light-sheet microscopy with a tunable lens,” *Opt. Express*, vol. 21, no. 18, pp. 21010–21026, Sep 2013.
- [3] S. Bhat, J. Ohn, and M. Liebling, “Motion-based structure separation for label-free high-speed 3-D cardiac microscopy,” *IEEE Trans. Image Process.*, vol. 21, no. 8, pp. 3638–3647, Aug 2012.
- [4] L. Wigström, L. Sjöqvist, and B. Wranné, “Temporally resolved 3D phase-contrast imaging,” *Magn. Reson. Med.*, vol. 36, no. 5, pp. 800–803, 1996.
- [5] M. Markl, A. Frydrychowicz, S. Kozerke, M. Hope, and O. Wieben, “4D flow MRI,” *J. Magn. Reson. Im.*, vol. 36, no. 5, pp. 1015–1036, 2012.
- [6] J.A. Jensen and P. Munk, “A new method for estimation of velocity vectors,” *IEEE Trans. Ultrason., Ferroelectr., Freq. Control*, vol. 45, 1998.
- [7] Y. Pu, X. Song, and H. Meng, “Off-axis holographic particle image velocimetry for diagnosing particulate flows,” *Exp. in Fluids*, vol. 29, no. 1, pp. 117–128, 2000.
- [8] F. Pereira, M. Gharib, D. Dabiri, and D. Modarress, “Defocusing digital particle image velocimetry: a 3-component 3-dimensional DPIV measurement technique. Application to bubbly flows,” *Exp. in Fluids*, vol. 29, no. 1, pp. 078–084, 2000.
- [9] X. Liu, K.Z. Abd-Elmoniem, M. Stone, E.Z. Murano, J. Zhuo, R.P. Gullapalli, and J.L. Prince, “Incompressible deformation estimation algorithm (IDEA) from tagged MR images,” *IEEE Trans. Med. Imag.*, vol. 31, no. 2, pp. 326–340, Feb 2012.
- [10] A. Falahatpisheh, G. Pedrizzetti, and A. Kheradvar, “Three-dimensional reconstruction of cardiac flows based on multi-planar velocity fields,” *Exp. in Fluids*, vol. 55, no. 11, 2014.
- [11] M. Arigovindan, M. Sühling, C. Jansen, P. Hunziker, and M. Unser, “Full motion and flow field recovery from echo doppler data,” *IEEE Trans. Med. Imag.*, vol. 26, no. 1, pp. 31–45, Jan 2007.
- [12] O. Skrinjar, A. Bistoquet, J. Oshinski, K. Sundareswaran, D. Frakes, and A. Yoganathan, “A divergence-free vector field model for imaging applications,” in *IEEE Int. Symp. Biomed. Imag.*, June 2009, pp. 891–894.
- [13] A.H. Squillacote, *The ParaView Guide: A Parallel Visualization Application*, Kitware, Inc., 3rd edition, 2008.
- [14] B.D. Lucas and T. Kanade, “An iterative image registration technique with an application to stereo vision,” in *Int. Joint Conf. Artificial Intel.*, 1981, pp. 674–679.
- [15] M.D. Abramoff, W.J. Niessen, and M.A. Viergever, “Objective quantification of the motion of soft tissues in the orbit,” *IEEE Trans. Med. Imag.*, vol. 19, no. 10, pp. 986–995, Oct 2000.